Cold collisions of O_2 with helium

John L. Bohn*
JILA and Department of Physics, University of Colorado, Boulder, Colorado 80309
(Received 23 February 2000; published 3 August 2000)

Collision cross sections between oxygen molecules and helium atoms are computed at translational energies between 0.1 K and 10.0 K, motivated by the recently demonstrated cooling of molecules by a helium buffer gas. Detailed calculations based on a rigid-rotor model demonstrate the differences among various isotopic combinations of oxygen atoms and also serve to illustrate resonant features unique to cold molecules. Comparisons of elastic versus spin-changing inelastic collision rates suggest that buffer-gas cooling is likely to be a widely applicable tool for producing cold molecular samples.

PACS number(s): 34.20.Cf, 34.50.−s, 05.30.Fk

I. INTRODUCTION

A. Background

Ultracold molecular gases are rapidly becoming a reality in a number of laboratories worldwide, and are being produced by a wide variety of techniques. The coldest molecular samples have thus far been produced by means of photoassociation (PA) [1–4]. In this case a sample of ultracold atoms is subjected to one or more PA lasers which serve to catalyze the combination of atom pairs into bound molecular states. The resulting molecules have nearly the same translational temperatures as the original atomic sample (as low as 100 nanoKelvin for molecules extracted from a Bose-Einstein condensate [4]). They are also rotationally cold owing to dipolar selection rules, but tend to be vibrationally quite hot. Careful selection of intermediate molecular levels may increase the likelyhood of producing vibrational ground states [5,6]. Vibrationally hot molecules pose a substantial theoretical challenge in understanding their vibrational relaxation [7].

Alternative methods for cooling molecules directly have included buffer-gas cooling (BGC) [8,9], Stark slowing [10,11], and expansions from moving jets [12]. These techniques have in common the population of molecules predominantly in their vibrational and rotational ground states, but so far exhibit fairly high translational temperatures. The lowest temperature so far reported is 0.3 K in a gas of CaH molecules that have been buffer-gas cooled and magnetically trapped by Doyle's group [13].

Theoretical understanding of molecular collisions at these temperatures is also of basic interest, for several reasons. (i) Cooling strategies, for example BGC, which has achieved sub-Kelvin temperatures, or forced evaporative cooling, which may be required to produce even lower temperatures, demand a detailed picture of elastic scattering. (ii) Magnetic trapping, and also electric field trapping of polar molecules, require molecular magnetic or electric dipole moments to be properly aligned relative to the trapping field. As is well known from magnetic trapping experiments for atoms, collisions can disrupt this alignment, and therefore collision rates need to be evaluated. (iii) Interesting collision phenomena can appear at temperatures below the rotational energy splittings of molecules, including types of Bose-condensed samples.

This paper examines a particular facet of cold atom-molecule scattering, namely, collisions between ^{3}He atoms and molecular oxygen. We choose to consider O_2 rather than the CaH that was trapped by Doyle's group because there already exists an accurate potential energy surface for the He-O_2 interaction [14]. We therefore anticipate that the computed collision rates have realistic magnitudes. One part of the work sets up a realistic model of this scattering as a preliminary to understanding cold molecule-molecule scattering in general, and to exhibit the rich resonant structure that is obtained. A second part discusses the resulting scattering rate constants from the point of view of BGC of oxygen. In this context, we extend the work of Ref. [15] to encompass various isotopomers (i.e., oxygen molecules composed of various isotopes of atomic oxygen). Qualitatively we find that all the isotopomers have roughly the same scattering properties above about 2 K, but that isotopomers other than $^{16}O_2$ and $^{18}O_2$ possess strongly suppressed spin-flip rates at lower temperatures. In particular, we will see that rate constants for He-$^{17}O_2$ collisions lie below 10^{-14} cm^3/sec at sub-Kelvin temperatures, in agreement with the rates estimated for He-CaH collisions [13].

B. Oxygen molecules—General considerations

The oxygen molecule is a natural candidate for magnetic trapping experiments, as it is one of the simplest paramagnetic diatomic species. It is moreover a molecule of intense chemical interest that would benefit from spectroscopic and collisional studies at ultralow temperatures. Molecular oxygen has in fact already been considered as a candidate for buffer gas cooling in [16], and has been slowed by a rotating jet [12]. As Ref. [16] pointed out, oxygen's prospects for collisional stability in a magnetic trap are colored by the nuclear spin statistics of the molecule.

We are concerned throughout this paper with the electronic ground state of oxygen, $^3\Sigma_g^-$. The molecule is also considered to be in its vibrational ground state $v=0$. For the homonuclear species $^{16}O_2$ and $^{18}O_2$, whose nuclei are identical spin-zero bosons, the quantum number N of molecular rotation is then restricted to even values [17]. By contrast,

*Email address: bohn@murphy.colorado.edu

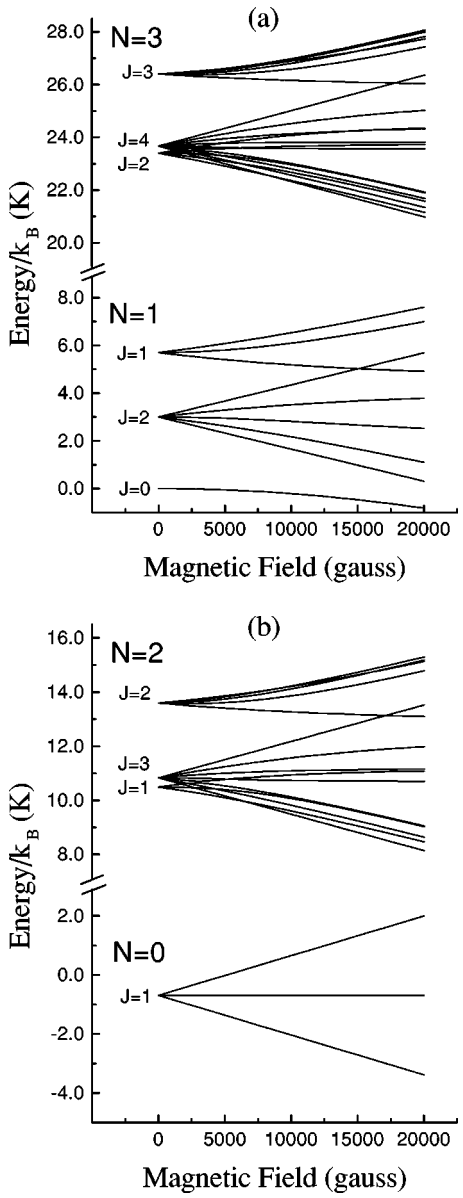

FIG. 1. The lowest-energy Zeeman levels of O_2, for odd-N (a) and even-N (b) rotational manifolds.

molecules consisting of two ^{17}O atoms, which have nuclear spin 5/2, can have either even or odd values of N, but not both at the same time: To the extent that the total nuclear spin I is conserved (as we assume here), the value of N is even for odd values of I and vice versa [17]. We therefore limit the discussions of this paper to the ''even-N'' and ''odd-N'' manifolds of molecular states. Note that for heteronuclear molecules, e.g., ^{16}O-^{18}O, these symmetry considerations no longer apply, and collisions can interconvert even and odd values of N. However, the rates for such processes are likely to be low, as discussed in Sec. III D.

To understand magnetic trapping it is essential to understand the behavior of the molecules in a magnetic field. The low-energy Zeeman levels of oxygen are displayed in Fig. 1 for both odd-N [18] and even-N [19] species. (Throughout this paper we report energies in units of Kelvin by dividing by the Boltzmann constant k_B. These units are related to the more familiar wave numbers via $1\ \mathrm{K}=0.695\ \mathrm{cm}^{-1}$.) The triplet electronic structure of the oxygen molecule ($S=1$) implies that the total spin $\mathbf{J}=\mathbf{N}+\mathbf{S}$ can have quantum number $J=N-1$, N, or $N+1$. In order to be trapped in the usual magnetic traps, a molecule must be in a weak-field-seeking state, i.e., one whose energy rises with increasing magnetic-field strength. Thus, for example, the states $|N,JM_J\rangle = |1,2\,2\rangle$ and $|1,2\,1\rangle$ are the lowest-lying trappable states of the odd-N manifold, while $|0,1\,1\rangle$ is the lowest-lying trappable state of the even-N manifold. These are the states on which we focus our attention below.

It is clear from Fig. 1 that for any trapped state there is an untrapped, strong-field-seeking Zeeman state at a lower energy. In a magnetic trap and at sufficiently low temperature, collisions with the buffer gas will therefore ultimately transfer the entire molecular population to untrapped spin states. These states are not merely untrapped but antitrapped, experiencing a force away from the trapping region. The time available for BGC is therefore limited and knowledge of the rate constants for spin-flipping collisions is essential to predicting the success of the buffer-gas process. Notice that, while nonvanishing gradients of the magnetic field are required to trap molecules, the value of the field itself vanishes in the center of Ref. [13]'s trap. Since this is where the molecules appear with highest density, most collisions of interest occur at small values of the field. The zero-field results computed below should thus serve as useful guidelines for experiments of the type of Ref. [13]. After deriving and computing the relevant rate constants in Secs. II and III, we return to the discussion of BGC in Sec. IV.

II. THE MODEL

This discussion follows Ref. [15] by focusing mainly on collision cross sections and rate coefficients in the energy range 0.1–10 K. This is an important energy range for experiments since the depth of the relevant magnetic trap is several K [13]. It is therefore in this range that cold molecular collision studies could begin in earnest. We disregard for now the molecular hyperfine interaction, since in $^{17}O_2$ the hyperfine splitting is of order mK, much smaller than the translational energies. We moreover compute the cross sections in zero magnetic field, as we are interested for now primarily in the magnitudes of cross sections as well as resonant features, which are of course present even in the $B=0$ limit.

A. The He-O_2 Hamiltonian

We begin with the potential-energy surface (PES) that describes the interaction between a helium atom and an oxygen molecule in its electronic and vibrational ground state. This surface has been computed by *ab initio* means by Cybulski *et al.*, using a supermolecule approach [14]. This reference approaches the problem by treating the molecule as a rigid rotor with the nuclei fixed at their known equilibrium separation. It then solves the electronic structure problem, generating a Born-Oppenheimer PES. The rigid rotor approximation should be quite good in the context of cold col-

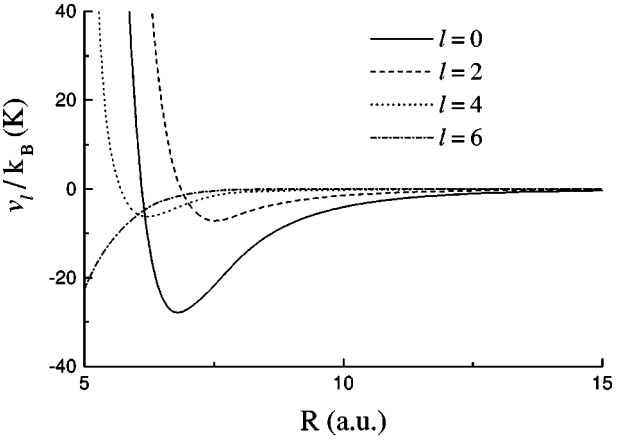

FIG. 2. The radial functions $v_l(R)$ used in the expansion of the potential energy surface [Eq. (1)]. Elastic scattering is dominated by the isotropic component $v_0(R)$ (solid line).

lisions since vibrational excitations of energy $>10^3$ K should be frozen out at the temperatures of interest. Cybulski *et al.* suggest that their variational calculation may underestimate the true depth of the PES by perhaps 20%; we therefore correct the nominal PES by multiplying it globally by a factor of 1.2. Reference [15] made a preliminary comparison of the nominal PES and the ''deepened'' one, finding differences mainly in the positions of resonance features but not in the overall magnitudes of cross sections.

As a first step in adapting the PES to a set of coupled-channel equations, we expand the PES into angular and radial functions:

$$V(R,\theta)=\sum_l v_l(R)P_l(\cos\theta). \tag{1}$$

In this expression R is the magnitude of the vector $\mathbf{R}$ extending between the atomic and molecular centers of mass, and θ is the angle that the molecule's axis makes with respect to $\mathbf{R}$. The functions $v_l(R)$ are radial expansion functions, and P_l stands for the Legendre polynomials. The end-over-end symmetry of homonuclear molecules restricts the sum in Eq. (1) to even values of l. For heteronuclear species there is no such restriction, however such a PES is beyond the scope of Ref. [14]. Figure 2 shows the different components $v_l(R)$ extracted from a fit to Ref. [14]'s PES. The largest contribution to anisotropy arises from the $l=2$ term.

The full multichannel calculation requires casting $V(R,\theta)$ in an appropriate angular momentum basis. Here we follow the model of atom-diatom scattering originally due to Arthurs and Dalgarno [20,21], modified to incorporate the electronic spin of the oxygen molecule. Namely, we express the Hamiltonian in a basis of total angular momentum,

$$\mathcal{J}=\mathbf{N}+\mathbf{S}+\mathbf{L}, \tag{2}$$

in terms of the molecule's mechanical rotation ($\mathbf{N}$), its electronic spin ($\mathbf{S}$), and the partial wave representing the rotation of the molecule and the He atom about their center of mass ($\mathbf{L}$). In an intermediate angular momentum coupling scheme we combine $\mathbf{N}$ and $\mathbf{S}$ to construct the total molecular spin $\mathbf{J}$.

Our basis for close-coupling calculations is then

$$|O_2(^3\Sigma_g^-, v=0)\rangle|He(^1S)\rangle|\{[(SN)J]L\}\mathcal{J}M\rangle. \tag{3}$$

At the collision energies of interest we assume that the oxygen electronic and vibrational states and the helium-atom states are preserved. Therefore we suppress the first two kets in Eq. (3) in what follows and focus on the molecular angular momentum states.

Evaluation of the PES (1) in the basis (3) involves rotating the Legendre functions P_l, which are referred to the $\mathbf{R}$ axis, into the laboratory frame to which the molecular spins and partial waves are ultimately referred. This is most easily accomplished using the spherical harmonic addition theorem,

$$P_l(\cos\theta)=\sum_m C_{lm}(\hat{R})^* C_{lm}(\hat{R}_{\rm mol}). \tag{4}$$

Here the C_{lm}'s are the normalized spherical harmonics (Ref. [22], Appendix IV). As above, $\hat{R}$ is the direction of the molecule-atom relative coordinate, and we introduce $\hat{R}_{\rm mol}$ as the orientation of the molecule's axis referred to the laboratory frame.

Recognizing the right-hand side of Eq. (4) as the scalar product of two tensor quantities, the evaluation of the relevant matrix elements reduces to an exercise in the Wigner-Eckart theorem. Reduced matrix elements of the scalar product can be evaluated starting from Eq. (5.13) of [22]. The final result is

$$\begin{aligned}\langle\{[(NS)J]L\}\mathcal{J}M|P_l(\cos\theta)|\{[(N'S)J']L'\}\mathcal{J}'\mathcal{M}'\rangle &= \delta_{\mathcal{J}\mathcal{J}'}\delta_{\mathcal{M}\mathcal{M}'}(-1)^{2J'+S+l+\mathcal{J}} \\ &\times\sqrt{[N][J][L][N'][J'][L']}\begin{Bmatrix} J & J' & l \\ L' & L & \mathcal{J}\end{Bmatrix} \\ &\times\begin{Bmatrix} J & J' & l \\ N' & N & S\end{Bmatrix}\begin{pmatrix} L & l & L' \\ 0 & 0 & 0\end{pmatrix}\begin{pmatrix} N & l & N' \\ 0 & 0 & 0\end{pmatrix},\end{aligned} \tag{5}$$

where $[N]=(2N+1)$, etc. Notice that Eq. (5) reduces to the Arthurs-Dalgarno model when $S=0$ [21].

The matrix element in Eq. (5) emphasizes the role of the anisotropy terms l in coupling different rotational states N and *simultaneously* different partial waves L. For homonuclear species with l even, the 3-j symbols in Eq. (5) indicate explicitly that the parity of both N and L is conserved in these collisions.

The rest of the scattering Hamiltonian is constructed easily in this basis. The atom-molecule relative kinetic energy is diagonal and has the form

$$-\frac{\hbar^2}{2\mu}\left[\frac{d^2}{dR^2}-\frac{L(L+1)}{R^2}\right], \tag{6}$$

after multiplying the wave function by R to remove first derivatives. Likewise the molecular fine structure, which

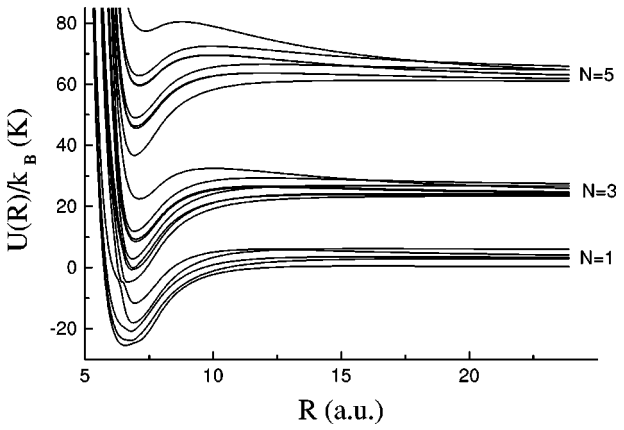

FIG. 3. A sample set of adiabatic curves, in this case for total angular momentum $\mathcal{J}=2$. In computing these curves only the values $N=1,3,5$ and $L=0,2,4,6,8$ are kept.

arises from the molecular rotation and spin-rotation coupling, is diagonal in this basis, at least at large R. We follow the common practice in the theory of cold atomic collisions and assert that this fine structure is R-independent. For $^{16}O_2$ we use the fine-structure constants determined in [18], while for $^{17}O_2$ we employ those determined in [19].

Figure 3 shows a typical set of adiabatic potential curves, in this case for $\mathcal{J}=2$. To generate this figure we include rotational channels $N=1,3,5$ and even partial waves $L=0-8$, which already imply 21 total channels in this case. This remark illustrates the relative richness of the scattering Hamiltonian here, as compared, for instance, to cold collisions of alkali-metal atoms. The total number of channels involved, even for a fixed value of $\mathcal{J}$, can be quite large, since both N and L can range in principle to infinity. However, truncation of the basis is usually quite straightforward at the low collision energies that we consider. In particular, rotational states up to $N=5$ and partial waves up to $L=10$ suffice for our present purposes. Thus the total number of channels in this study, including all values of $\mathcal{J}$, is 555. Working in a basis of total $\mathcal{J}$ guarantees that no fixed-$\mathcal{J}$ block of the Hamiltonian contains more than 32 channels, at least in the zero-magnetic-field limit.

B. Evaluating cross sections

Once the Hamiltonian is in place, the coupled-channel equation is solved subject to scattering boundary conditions to yield scattering matrices. Since we assume zero magnetic field, the total angular momentum $\mathcal{J}$ is a good quantum number, and moreover the results are independent of the laboratory projection $\mathcal{M}$ of total angular momentum. The resulting total-$\mathcal{J}$ scattering matrices, of the form

$$\langle [(NS)J]L|S(\mathcal{J})|[(N'S)J']L'\rangle, \tag{7}$$

nevertheless allow for changing both the molecule's internal state and the partial wave during a collision.

The molecular quantum numbers of greatest interest in the context of magnetic trapping are naturally the magnetic quantum numbers. The scattering matrices (7) are easily converted to the appropriate basis by standard angular momentum algebra:

$$\begin{aligned}\langle (NS)JM_J LM_L|S|(N'S)J'M_J'L'M_L'\rangle &= \sum_{\mathcal{J}} \langle JM_J LM_L|\mathcal{J}M\rangle \\ &\times \langle [(NS)J]L|S(\mathcal{J})|[(N'S)J']L'\rangle \\ &\times \langle \mathcal{J}M|J'M_J'L'M_L'\rangle. \end{aligned} \tag{8}$$

Note that in general all the quantum numbers N, J, M_J, L, and M_L are subject to change in a collision.

The next issue is to transform the scattering matrices into meaningful cross sections. For a magnetically trapped gas it is the quantization axis that selects a preferred laboratory axis, as opposed to the collision axis that would set the direction in a beam experiment. Consequently, we construct state-to-state cross sections $\sigma_{N,JM_J\to N',J'M_J'}$ averaged over all incident directions.

To this end we follow Mott and Massey [23], denoting the molecular state $|N,JM_J\rangle$ by the collective symbol $|p\rangle$. An incident plane wave with wave vector $\vec{k}_p$ and having molecules in state p is then

$$\exp(i\vec{k}_p\cdot\vec{R})|p\rangle = 4\pi\sum_{LM_L} i^L Y^*_{LM_L}(\hat{k}_p) j_L(k_pR) Y_{LM_L}(\hat{R})|p\rangle, \tag{9}$$

which in the limit of large R becomes

$$\frac{4\pi}{2ik_pR}\sum_{LM_L} i^L Y^*_{LM_L}(\hat{k}_p) \times [e^{i(k_pR-L\pi/2)} - e^{-i(k_pR-L\pi/2)}] Y_{LM_L}(\hat{R})|p\rangle. \tag{10}$$

The complete (incident plus scattered) wave function in the limit of large R is given by [23]

$$\begin{aligned}&\frac{4\pi}{2i\sqrt{k_p}R}\sum_{LM_L} i^L Y^*_{LM_L}(\hat{k}_p) \sum_{p'L'M_L'} \frac{1}{\sqrt{k_{p'}}} Y_{L'M_L'}(\hat{R})|p'\rangle \\ &\times [-\delta_{pp'}\delta_{LL'}\delta_{M_LM_L'} e^{-i(k_{p'}R-L'\pi/2)} \\ &+ \langle pLM_L|S|p'L'M_L'\rangle e^{i(k_{p'}R-L'\pi/2)}]. \end{aligned} \tag{11}$$

As is conventionally done, we can rearrange this expression to separate, in the large-R limit, the incident wave and the scattered wave,

$$\exp(i\vec{k}_p\cdot\vec{R}) + \sum_{p'} f_{p'}(\theta,\phi)\frac{\exp(ik_{p'}R)}{R}|p'\rangle. \tag{12}$$

Here $f_{p'}$ denotes the channel-dependent scattering amplitude as a function of the scattering angles θ and ϕ. Its form in terms of the scattering matrix is

$$f_{p'}(\theta,\phi)=\frac{4\pi}{2i\sqrt{k_p k_{p'}}}\sum_{LM_L L'M'_L} i^L Y^*_{LM_L}(\hat{k}_p) \times\langle pLM_L|S-I|p'L'M'_L\rangle i^{-L'}Y_{L'M'_L}(\theta,\phi)|p'\rangle, \tag{13}$$

where I denotes the identity matrix.

To determine the scattering cross section for transforming from channel p to channel p' for a particular incident direction $\hat{k}_p$, we must integrate over the angular coordinates of the scattered wave:

$$\sigma_{p\to p'}(\hat{k}_p)=\int d\phi d(\cos\theta)\frac{k_{p'}}{k_p}|f_{p'}|^2 \tag{14}$$

The total state-to-state cross section of interest further requires an appropriate directional average over incident directions $\hat{k}_p$, as noted above. Assuming that the incident directions are distributed isotropically, the desired cross section becomes

$$\sigma_{N,JM_J\to N',J'M'_J}=\frac{\pi}{k^2_{N,JM_J}}\sum_{LM_L L'M'_L}|\langle N,JM_J LM_L| \times S-I|N',J'M'_J L'M'_L\rangle|^2. \tag{15}$$

We have here resubstituted the molecular quantum numbers N,JM_J for the index p. Notice that the sums over partial wave quantum numbers in this expression are incoherent, resulting from the integration over initial as well as final directions. Had we fixed an incident direction for the collision, we would have found a coherent sum over the incident quantum numbers [23]. Finally, state-to-state rate coefficients are given by

$$K_{N,JM_J\to N',J'M'_J}=v_{N,JM_J}\sigma_{N,JM_J\to N',J'M'_J}, \tag{16}$$

where v_{N,JM_J} is the relative velocity of the collision partners before the collision.

III. RESULTS

A. General features

This paper only considers the helium isotope ^{3}He, which is of greater experimental relevance because its higher vapor pressure at sub-Kelvin temperatures makes it a more suitable buffer gas than ^{4}He. We do, however, consider various isotopomers of O_2. The different possibilities are fairly well typified by the examples of $^{16}O_2$ and $^{17}O_2$, if we bear in mind three issues.

One issue is the influence of uncertainties in the PES on the final result. In the case of the He-O_2 PES of Cybulski, this is not a serious issue since their stated uncertainty is only 20% of the total well depth. As illustrated in Ref. [15], this uncertainty does not much affect the magnitudes of rates for elastic and spin-changing collisions, although it does have the effect of moving resonance positions. That is, the PES is sufficiently shallow that not much phase is accumulated between the scattering partners; small changes in the PES do not introduce much overall phase change. Resonances are particularly sensitive to phases and are therefore more strongly affected. In this work we have multiplied Cybulski *et al.*'s PES uniformly by a factor of 1.2 to be ''on the safe side.''

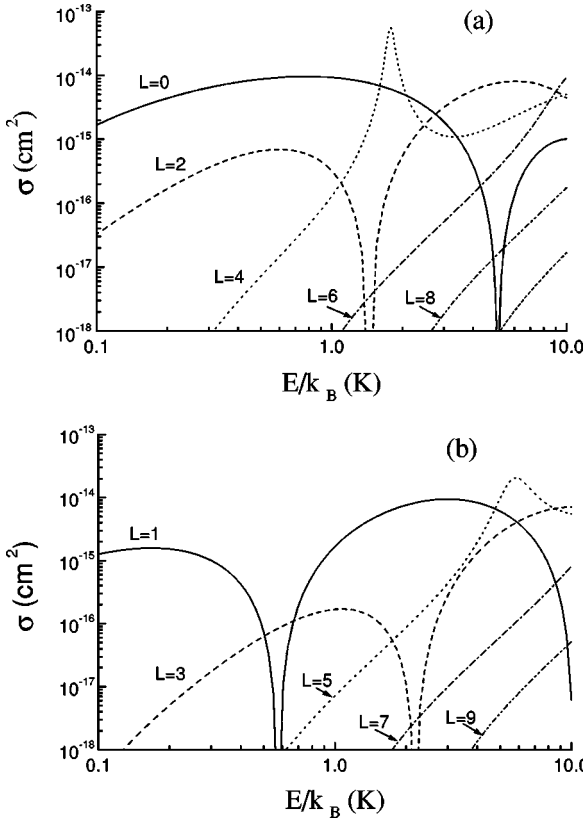

FIG. 4. Elastic scattering cross sections σ_{el} versus energy for the isotropic potential curve $v_0(R)$. The cross sections are divided into even (a) and odd (b) partial waves L.

Another issue is the influence of the different reduced masses of the He-O_2 pair as the oxygen isotopes are varied. Again this introduces only small effects in the final cross sections, since the reduced masses change only very slightly. For example, the *s*-wave scattering length for the isotropic potential $v_0(R)$ is -1.2 a.u. for $^{16}O_2$ and moves only to -1.5 a.u. for $^{17}O_2$. Accordingly, we adopt the following strategy for reporting results. For the odd-N manifolds in Sec. III B we perform the calculations with the correct He-$^{16}O_2$ reduced mass since this isotopomer typifies the odd-N states. For the even-N manifolds in Sec. III C we use the ^{3}He-$^{17}O_2$ reduced mass.

A third issue is that the PES is very nearly isotropic, meaning that elastic scattering is largely determined by the lowest-order term $v_0(R)$. For reference we plot in Fig. 4 the elastic scattering cross sections versus collision energy E for even and odd partial waves L for a single channel scattering in the potential $v_0(R)$. In light of the remarks above, we can say that these are ''typical'' cross sections for the He-O_2 system, although details may change somewhat. A main feature illustrated by this figure is that partial waves above L

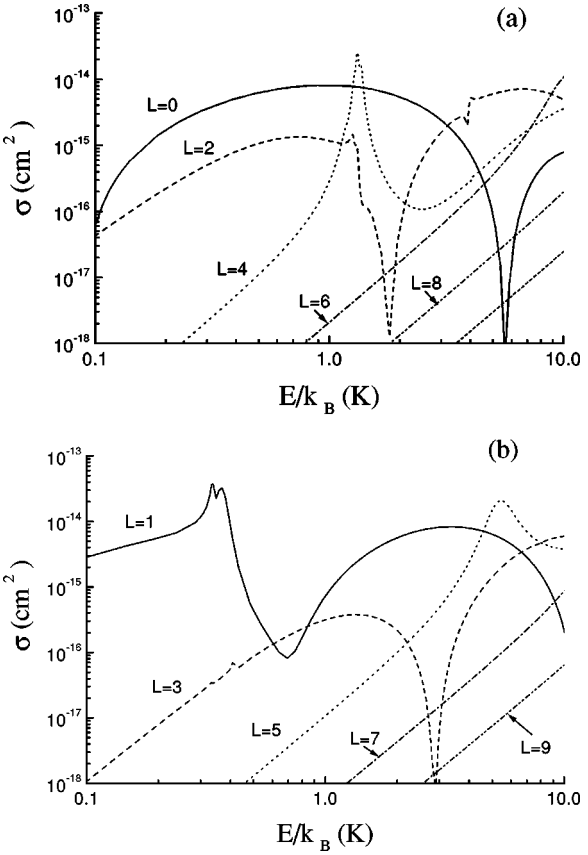

FIG. 5. Elastic partial-wave cross sections for the odd-N manifold. Shown are the fixed-L cross sections defined in Eq. (17) for $^{16}O_2$ molecules in their magnetically trapped $|N,JM_J\rangle=|1,2\ 2\rangle$ state. As in Fig. 4, these cross sections are separated into even-L (a) and odd-L (b) contributions.

$=6$ contribute only weakly to scattering in the energy range shown. A second feature is the appearance of shape resonances in the partial waves $L=4$ at $E\approx 1.8$ K and $L=5$ at $E\approx 5.8$ K. These resonances are relevant to the discussion below.

B. The odd-N manifold of states

In this subsection we focus on the $^{16}O_2$ molecule as exemplifying scattering in the odd-N manifold. The expression in Eq. (15) for the cross section requires an incoherent sum over incident and final partial waves. Therefore, it makes sense to extract a set of partial wave cross sections, given by

$$\sigma^{L}_{N,JM_J\to N',J'M'_J}=\frac{\pi}{k^2_{N,JM_J}}\sum_{M_LM'_L}|\langle N,JM_JLM_L|\times S-I|N',J'M'_JLM'_L\rangle|^2. \qquad (17)$$

These cross sections are shown in Fig. 5 for the trappable state $|N,JM_J\rangle=|1,2\ 2\rangle$. They are separated into even (a) and odd (b) partial waves L, which remain distinct for homonuclear species. Overall these curves are quite similar to those in Fig. 4, a testimony to the dominance of isotropy to the collisions. The total cross sections in Eq. (15) of course require sums over L-changing contributions; however, these corrections are far smaller than the fixed-L contributions shown.

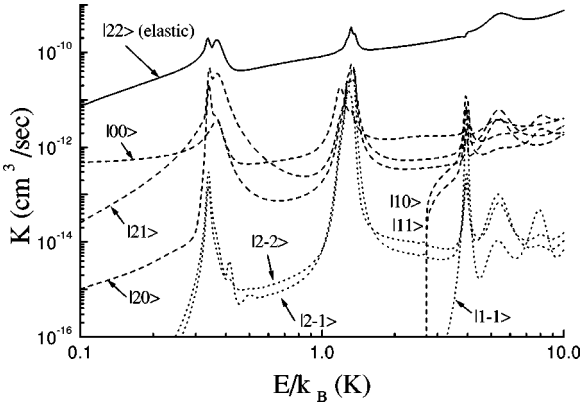

FIG. 6. Rate constants as defined by Eq. (16) for collisions with $^{16}O_2$ molecules initially in their $|N,JM_J\rangle=|1,2\ 2\rangle$ state. For each curve the final state is indicated.

The cross sections in Fig. 5 differ from those in Fig. 4 in that they reflect couplings due to anisotropies in the PES and therefore give rise to additional resonance features. For even partial waves [Fig. 5(a)] the shape resonance in the $L=4$ partial wave has contaminated the $L=2$ partial wave. It has moreover reasserted itself at a collision energy of $E\approx 3.9$ K. In this context the resonance represents a molecule that spin-flips from a $J=2$ state to a $J=1$ state and then becomes trapped behind the $L=4$ partial wave barrier correlating to the $J=1$ threshold. It is therefore a compound resonance of both Feshbach and shape character. In odd partial waves we see an extra resonant feature predominantly in the $L=1$ partial wave at a collision energy of $E\approx 0.35$ K. This is a Feshbach resonance belonging to an $L=3$ bound state lying below the $J=1$ threshold.

Figure 6 shows the rate constants as defined by Eq. (16) for producing all the possible final molecular states from an initial $|1,2\ 2\rangle$ state of the molecule. Notice that states with $J=1$ only become energetically available above $E=2.7$ K [compare Fig. 1(a)]. Away from any resonances some general features are apparent in the rate constants. Elastic scattering, which does not change M_J, is by far the most likely outcome of a collision, with rate constants between 10^{-11} and 10^{-9} cm^3/sec. Next likely are those processes in which the final value of M_J is either 0 or 1, with rate constants more on the order of 10^{-12} cm^3/sec (dashed lines). The least likely processes are those that yield $M_J=-1$ or -2 in the final state and have rate constants near 10^{-14} cm^3/sec (dotted lines).

These general trends are interpreted as follows. A process that changes M_J by one or two units requires a change in the partial wave of at least two units to conserve angular momentum. By contrast, a process that changes M_J by three or four units requires changing L by at least four units and is therefore second order in the anisotropy. The results in Fig. 6 illustrate that for this PES the anisotropy costs approximately two orders of magnitude in rate constant for every two units of angular momentum change in partial wave.

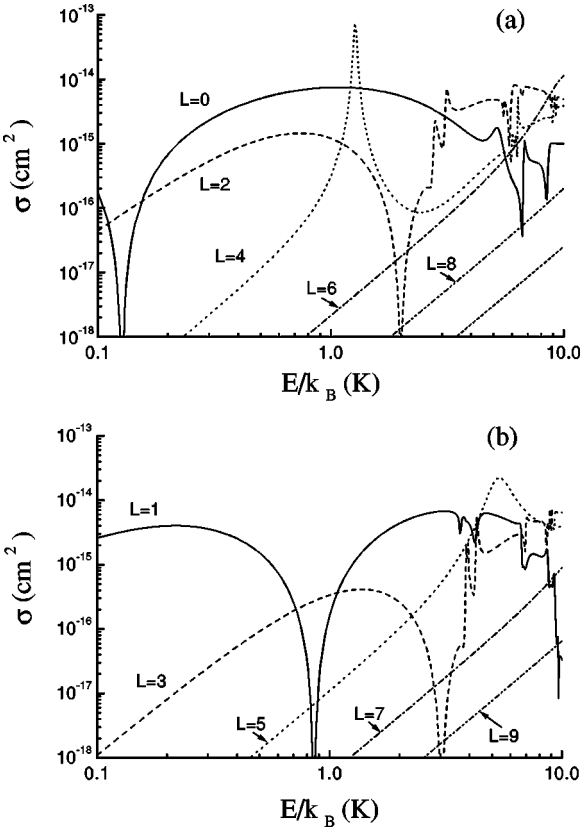

FIG. 7. Elastic partial-wave cross sections for the even-N manifold. Shown are the fixed-L cross sections defined in Eq. (17) for $^{17}O_2$ molecules in their $|N,JM_J\rangle=|0,1\,1\rangle$ state. As in Fig. 4, these cross sections are separated into even-L (a) and odd-L (b) contributions.

Another trend is the low-energy behavior of the rates, which is influenced by the Wigner threshold law. Namely, the rate constant to produce $|1,0\,0\rangle$ states becomes nearly constant at low energies. It does not experience threshold behavior in the final state, since at least 3 K of kinetic energy is liberated in the $J=2\rightarrow J=0$ transition [see Fig. 1(a)]. Consequently, the rate for this process remains at the same high value it has at higher collision energies. Collisions having $J=2$ in the final state are near threshold in the exit channel, and therefore are suppressed.

Near resonance these trends do not hold: Resonant collisions can produce spin-changing rates nearly comparable to elastic scattering rates.

C. The even-N manifold of states

This section focuses on $^{17}O_2$ molecules and in particular those with odd values of total nuclear spin I. This constraint demands that N take only even values [17]. Note that for even I we would recover the odd-N manifold, but by the arguments given above the results are qualitatively the same as the $^{16}O_2$ results in Sec. III B. We do not reproduce them here.

Figure 7 illustrates the elastic partial wave cross sections [Eq. (17)] for the even-N manifold, assuming an incident state $|0,1\,1\rangle$. Again the gross features of these cross sections

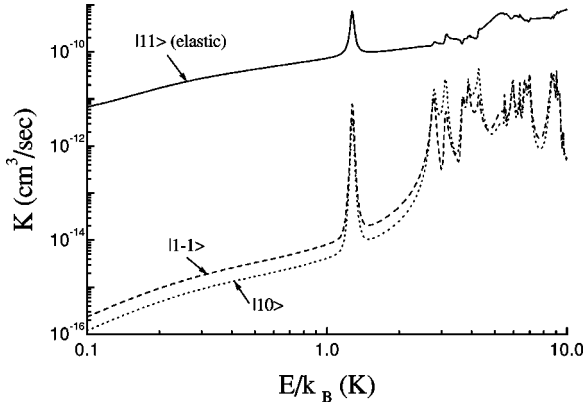

FIG. 8. Rate constants as defined by Eq. (16) for collisions with $^{17}O_2$ molecules initially in their $|N,JM_J\rangle=|0,1\,1\rangle$ state. For each curve the final state is indicated.

resemble those of the isotropic cross sections in Fig. 4, including shape resonances in the $L=4$ and $L=5$ partial waves. There are, however, far more resonances in the energy range $2\ \mathrm{K}<E<10\ \mathrm{K}$ than in the odd-N case above. This is because the next accessible rotational level $N=2$ lies only ≈ 11 K higher in energy (Fig. 1), meaning that the quasibound states lying below the $N=2$ threshold act as Feshbach resonances in the energy range we are considering. For example, the lowest of these resonances occurs at $E=3$ K. This is approximately the energy difference between the thresholds $N=2$, $J=1$, and $N=0(11\ \mathrm{K})$, less the binding energy of the s-wave bound state of $v_0(R)$ (7.2 K). There is an additional small energy shift due to coupling with the closed $N=5$ rotational channels. Similarly, the remaining resonance features can be roughly assigned.

These resonances are foreign to cold atomic collisions since they arise from the rearrangement of mechanical rotational energy. At low enough temperatures, translational kinetic energy is transformed by the anisotropy of the PES into rotational energy, effectively binding the molecules transiently together. This type of resonance should be ubiquitous in cold molecular collisions because the enormous number of internal molecular states leads to an equally large number of resonant states. For collisions between two molecules, the resonances will occur with even higher densities. Moreover, they are likely to appear even at zero collision energy, since in general the PES's are deeper. Thus resonances are certain to play a dominant role in cold molecule collisions, more so than in the case of cold atoms.

Figure 8 shows the elastic and inelastic rate constants for $^{17}O_2$. Recall that there are only two energetically allowed spin-changing exit channels, namely, $|N,JM_J\rangle=|0,1-1\rangle$ and $|0,1\,0\rangle$ (Fig. 1). The elastic rate constants are approximately the same as for the odd-N manifold, as expected from the general uniformity of elastic scattering. The spin-changing inelastic rates are also comparable in magnitude above ~ 2 K in collision energy. However, the inelastic rates are strongly suppressed to below 10^{-14} cm^3/sec at lower energies. This suppression is a consequence of the exit channels being degenerate with the entrance channel, i.e., the

same suppression as described above for the $J=2$ exit channels. Remarkably, this suppression makes the rates comparable to the empirical rates estimated in the CaH experiment [13].

D. Heteronuclear molecules

The preceding sections have dealt with oxygen molecules possessing rotational quantum numbers N of a fixed parity. This requires a homonuclear molecule along with some symmetry, for example a fixed value of I. For heteronuclear oxygen molecules no such restriction exists and even and odd values of N could intermix in collisions. However, we argue here that the rates for doing so are likely far smaller than the rates we have already computed.

For concreteness, let us consider the molecule ^{16}O-^{18}O. The ability to mix N's of different parity arises from breaking the end-over-end symmetry of the molecule, i.e., it requires there to be a difference in electronic energies between the two configurations He-^{16}O-^{18}O and He-^{18}O-^{16}O. This would in turn add terms with odd values of l in the expansion (1). Such terms are not present in the PES of Cybuslki *et al.*, who invoke a Born-Oppenheimer approximation. In other words, collisions that change the parity of N would be sensitive probes of nonadiabatic effects in the PES. Cold collisions of molecules ought to probe these effects with unprecedented precision.

As to the rates of the processes that change the parity of N, consider the following. The additional term $v_1(R)$ in the PES would arise purely from an isotope effect, meaning that its magnitude would be something like 10^{-3} of the isotropic part $v_0(R)$. However, we know already that the existing anisotropy which drives transitions, $v_2(R)$, is roughly comparable to the isotropic part (Fig. 2). Thus collisions that change the parity of N ought to be suppressed relative to those that preserve the parity by a factor of roughly $(10^{-3})^2$. They are therefore negligible relative to the rates we have computed above. Given these considerations, along with those in Sec. III A, we conclude that the rate constants given above are fairly representative of the dominant loss processes for *all* isotopomers of oxygen in collisions with ^{3}He atoms.

IV. DISCUSSION

The conclusions about atom-molecule collision rates obtained above can of course be tested in the buffer-gas cooled environment [13]. As has long been the case in cold atom studies, experimental corroboration is essential for fine-tuning the PES [24]. As an example of an experiment that would be immediately useful, consider preparing an isotopic mixture containing both ^{16}O and ^{18}O atoms of known relative abundances and rapidly cooling the resulting three isotopomers to subKelvin temperatures. If the populations of each isotopomer were separately monitored, there would result three characteristic time scales: (i) a very rapid depletion of $^{16}O_2$ and $^{18}O_2$ from the magnetic trap; (ii) a much slower depletion of ^{16}O-^{18}O molecules in their $N=0$, $J=1$ states (with rates comparable to those in Fig. 8); and (iii) a still slower conversion of ^{16}O-^{18}O molecules from their $N=1$ to their $N=0$ states. This last process would have to be disentangled from the more rapid $|1,2\,2\rangle \rightarrow |1,0\,0\rangle$ losses.

Comparison of time scales (i) and (ii) over a range of temperatures should elucidate corrections to the model we have proposed. In particular, note that we have so far altered the PES of Ref. [14] by multiplying it by a global constant. This constant, 1.2 in the present paper, accounts for the estimated discrepancy between the calculated and the ''true'' well depth. However, there is no reason that this discrepancy is the same factor everywhere. Put another way, it is possible that we have to correct the individual contributions $v_l(R)$ separately, much as the singlet and triplet potentials need to be fine-tuned separately in cold alkali-metal atom collisions. Only experiments will settle this issue. With this background information in hand, additional measurements of time scale (iii) would sensitively probe nonadiabatic effects.

Equally importantly, we are now able to draw tentative conclusions about the BGC process itself as an intermediate step toward producing large density samples of ultracold molecules. Roughly, for cooling to be effective the rate of elastic, rethermalizing collisions $K_{\rm el}$ must exceed the rate of spin-changing, lossy collisions $K_{\rm loss}$ by at least an order of magnitude [15]. Using this criterion, we can see from Fig. 8 that even-N oxygen molecules are quite robust against collisional losses, at least at collision energies below 2 K, where $K_{\rm el}/K_{\rm loss}\approx 10^4$. For the odd-$N$ manifold, by contrast, we have $K_{\rm el}/K_{\rm loss}\approx 10^2$. Thus while odd-$N$ species are probably also coolable by buffer-gas loading [15], they are less appealing for initial studies. This assumption has already been made in Ref. [16]; we have now quantified it by estimating the ratios of collision rates.

The suppression of lossy collisions for the even-N states arises partly from the anisotropy of the PES and partly from the degeneracy (at zero magnetic field) of the incident and spin-changing channels. The degeneracy in turn relies on the lowest-energy spin state having a nonzero spin [as in Fig. 1(b)]. This is the case in the vast majority of paramagnetic molecules—the $J=0$ ground state of $^{16}O_2$ is an accident of symmetry [17]. Therefore, we expect the even-N result $K_{\rm loss}\approx 10^{-14}$ cm^3/sec at low temperatures to be a ''representative'' value. By contrast, the odd-N value $K_{\rm loss}\approx 10^{-12}$ cm^3/sec is likely anomalously large. Indeed, the value 10^{-14} cm^3/sec is consistent with the upper limit estimated experimentally for He-CaH collisions in a 0.3 K gas [13]. Naturally, this should not be construed as representing ''agreement between theory and experiment,'' since the numbers pertain to two different physical systems. Nevertheless, the low rates are compelling and may speak to the efficiency of the buffer-gas-cooling enterprise as a whole.

One final word of caution is in order: the suppression enjoyed by the even-N manifold may disappear in the presence of a magnetic field, which splits the degeneracy of the thresholds. Magnetic-field dependence is beyond the scope of this paper, but we can estimate the scale of the effect. When the difference between the $|N,JM_J\rangle=|0,1\,1\rangle$ and

$|0,1-1\rangle$ thresholds becomes ≈ 2 K, the suppression should vanish since the loss rates climb back to 10^{-12} cm^3/sec (Fig. 8). This difference occurs at field values of $B \approx 7500$ G [Fig. 1(b)]. Since realistic trapping fields reach as high as 30 000 G [13], this possibility must be considered. These remarks point to the need to extend the present work to incorporate nonzero magnetic fields and to construct realistic sets of rate equations.

ACKNOWLEDGMENTS

This work was supported by the National Science Foundation.

[1] A. Fioretti *et al.*, Phys. Rev. Lett. **80**, 4402 (1998).
[2] T. Takekoshi, B.M. Patterson, and R.J. Knize, Phys. Rev. Lett. **81**, 5105 (1998); Phys. Rev. A **59**, R5 (1999).
[3] A.N. Nikolov *et al.*, Phys. Rev. Lett. **82**, 703 (1999).
[4] R. Wynar *et al.*, Science **287**, 1016 (2000).
[5] Y.B. Band and P.S. Julienne, Phys. Rev. A **51**, R4317 (1995).
[6] A.N. Nikolov *et al.*, Phys. Rev. Lett. **84**, 246 (2000).
[7] N. Balakrishnan, R.C. Forrey, and A. Dalgarno, Phys. Rev. Lett. **80**, 3224 (1998); R.C. Forrey, V. Kharchenko, N. Balakrishnan, and A. Dalgarno, Phys. Rev. A **59**, 2146 (1999); R.C. Forrey *et al.*, Phys. Rev. Lett. **82**, 2657 (1999).
[8] J.M. Doyle, B. Friedrich, J. Kim, and D. Patterson, Phys. Rev. A **52**, R2515 (1995).
[9] J.D. Weinstein *et al.*, J. Chem. Phys. **109**, 2656 (1998).
[10] H.L. Bethlem, G. Berden, and G. Meijer, Phys. Rev. Lett. **83**, 1558 (1999).
[11] J.A. Maddi, T.P. Dineen, and H. Gould, Phys. Rev. A **60**, 3882 (1999).
[12] M. Gupta and D. Herschbach, J. Phys. Chem. A **103**, 10 670 (1999).
[13] J.D. Weinstein *et al.*, Nature (London) **395**, 148 (1998).
[14] S.M. Cybulski *et al.*, J. Chem. Phys. **104**, 7997 (1996).
[15] J. L. Bohn, Phys. Rev. A **61**, 040702 (2000).
[16] B. Friedrich *et al.*, J. Chem. Soc., Faraday Trans. **94**, 1783 (1998).
[17] M. Mizushima, *The Theory of Rotating Diatomic Molecules* (Wiley, New York, 1975), p. 170.
[18] M. Tinkham and W.P. Strandberg, Phys. Rev. **97**, 937 (1955); **97**, 951 (1955).
[19] G. Cazzoli and C. Degli Esposti, Chem. Phys. Lett. **113**, 501 (1985).
[20] A.M. Arthurs and A. Dalgarno, Proc. R. Soc. London, Ser. A **256**, 540 (1960).
[21] M. S. Child, *Molecular Collision Theory* (Dover Publications, Mineola, 1996), p. 100.
[22] D. M. Brink and G. R. Satchler, *Angular Momentum*, 3rd ed. (Clarendon Press, Oxford, 1993).
[23] N. F. Mott and H. S. W. Massey, *The Theory of Atomic Collisions*, 3rd ed. (Clarendon Press, Oxford, 1965), Chap. XIV.
[24] J. Weiner, V.S. Bagnato, S. Zilio, and P.S. Julienne, Rev. Mod. Phys. **71**, 1 (1999).